Sustained State-Independent Quantum Contextual Correlations from a Single Ion

F. M. Leupold, M. Malinowski, C. Zhang, V. Negnevitsky, A. Cabello, J. Alonso, and J. P. Home

Phys. Rev. Lett. **120**, 180401 — Published 4 May 2018

DOI: 10.1103/PhysRevLett.120.180401

Sustained state-independent quantum contextual correlations from a single ion

F. M. Leupold, M. Malinowski, C. Zhang, V. Negnevitsky, J. Alonso,* and J. P. Home†
Institute for Quantum Electronics, ETH Zürich, Otto-Stern-Weg 1, 8093 Zürich, Switzerland

A. Cabello
Departamento de Física Aplicada II, Universidad de Sevilla, 41012 Sevilla, Spain

We use a single trapped-ion qutrit to demonstrate the quantum-state-independent violation of non-contextuality inequalities using a sequence of randomly chosen quantum non-demolition projective measurements. We concatenate 53 million sequential measurements of 13 observables, and unambiguously violate an optimal non-contextual bound. We use the same dataset to characterize imperfections including signaling and repeatability of the measurements. The experimental sequence was generated in real time with a quantum random number generator integrated into our control system to select the subsequent observable with a latency below 50 µs, which can be used to constrain contextual hidden-variable models that might describe our results. The state-recycling experimental procedure is resilient to noise and independent of the qutrit state, substantiating the fact that the contextual nature of quantum physics is connected to measurements and not necessarily to designated states. The use of extended sequences of quantum non-demolition measurements finds applications in the fields of sensing and quantum information.

Two measurements are said to be compatible when their outcome statistics for any given input state are indistinguishable from the individual statistics extracted from a joint measurement on that state. In classical theories, outcomes of measurements are consistent with each result having a pre-existing value, independent of which other compatible measurements are performed. Quantum Mechanics (QM) is bound by different rules, resulting in stronger correlations between the outcomes of compatible observables than are possible in classical theories. This feature, which is known as contextuality, has been linked to the power of quantum computation [1–5] and to reliable communication protocols [6, 7], and its most famous manifestation is Bell non-locality [8]. In this sense, the violation of a Bell inequality demonstrates contextuality. However, non-locality requires composite systems in entangled states. A more general result is that of Kochen and Specker [9], who showed that any state of any quantum system in a Hilbert space of dimension greater than 2 can be used to reveal contextuality.

In a similar fashion to a Bell-inequality, the contextuality of QM can be shown through the violation of a number of inequalities, which have been derived for systems of various Hilbert space dimension. Such inequalities can be split into those which are violated for a given input state [10, 11], and those for which the violation is input-state independent [12, 13]. State-Independent-Contextuality (SIC) tests have been performed using a number of systems [14–22], but thus far they all used the following approach: i) prepare an input state, ii) measure multiple observables. This was repeated for each of a finite number of input states, and using all combinations of observables required for the test. Measurements on each observable can either be carried out simultaneously or sequentially [23], with the sequential approach being the most popular.

An alternative proposal [24] is to perform a SIC test using sequences of ideal Quantum Non-Demolition (QND) projective measurements (which in the context of general probabilistic theories are known as sharp measurements [43]). Each measurement is performed on the state into which the system was projected by the previous measurement. When executed in this manner, contextuality tests intrinsically sustain the generation of quantum correlations, which can be used to generate and certify continuous strings of random numbers [26, 27].

In this Letter, we demonstrate SIC sustainable in time using state-recycling over a sequence of 53 million measurements. To that end we have adopted: i) the simplest system featuring SIC, a three-level quantum system or qutrit [9, 28], ii) the smallest set of elementary quantum measurements needed for SIC, namely, the Yu-Oh set with 13 observables [13, 29, 30], and iii) the original Yu-Oh and an optimal witness of SIC [31]. Our results violate the bounds imposed by non-contextual hidden-variable models. We use a commercial Quantum Random Number Generator (QRNG) to create the sequence of measured observables in real time. This places constraints on contextual hidden-variable models attempting to explain our results, which must cover the behavior not only of the qutrit but also of the QRNG [32]. We quantify the unsharpness and incompatibility (or signaling, see [33]) of our measurements by extracting high-order correlators from the dataset.

The 13 dichotomic ("yes-no") observables or "rays" in the Yu-Oh set [13] are of the form $A_v = I - 2P_v$, where I is the identity, P_v is the normalized projection operator onto a vector $|v\rangle = a\,|0\rangle + b\,|1\rangle + c\,|2\rangle$, and $\{|0\rangle, |1\rangle, |2\rangle\}$ form a qutrit basis. Since the eigenvalues of P_v are 0 and 1, ray measurements result in values $+1$ and -1. The 13 vectors $|v\rangle$ with real-valued coefficients (a, b, c) are defined by points on the surface of a cube in a three-dimensional Hilbert space (FIG. 1a, TABLE I). Two rays are compatible if the corresponding vectors are orthogonal. This can be visualized in an orthogonality graph (FIG. 1b) by drawing all vectors from the set $V = \left\{y_k^\sigma, h_\alpha, z_k | k = 1, 2, 3; \sigma = \pm; \alpha = 0, 1, 2, 3\right\}$ as vertices and linking vertices of compatible rays. In this notation, z_k are the basis states, y_k are superpositions of two basis states, and h_k are superpositions of all three. In total, there are 24 edges in the graph, representing the 24 compatible pairs

* alonso@phys.ethz.ch
† jhome@phys.ethz.ch

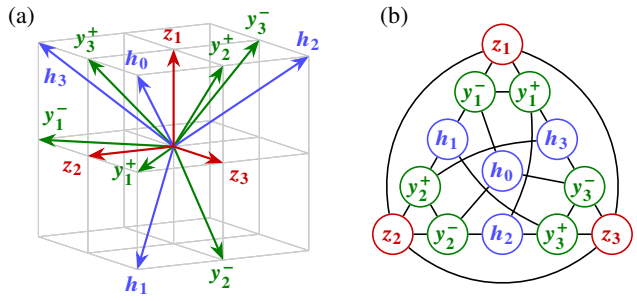

FIG. 1. (color online) Observables and compatibility relations between the observables for the Yu-Oh set. (a) The 13 rays are represented by vectors in a three-dimensional real Hilbert space. Their directional components are listed in TABLE I. (b) The orthogonality relationships between the rays determine a graph with 13 vertices and 24 edges between compatible rays.

$(u, v) \in E$ with $P_u P_v = 0$ (each edge is counted only once).

Besides the original Yu-Oh witness [13]

$$\langle \chi_{\rm YO} \rangle = \sum_{v \in V} \langle A_v \rangle - \sum_{(u,v)\in E} \frac{1}{2} \langle A_u A_v \rangle , \tag{1a}$$

we use the optimal SIC witness opt3 for which the QM and classical predictions differ maximally [31]

$$\begin{aligned} \langle \chi_{\rm opt3} \rangle = & \sum_{v \in V_h} 2 \langle A_v \rangle + \sum_{v \in V \setminus V_h} \langle A_v \rangle \\ & - \sum_{(u,v)\in E\setminus C_2} 2 \langle A_u A_v \rangle - \sum_{(u,v)\in C_2} \langle A_u A_v \rangle \\ & - \sum_{(u,v,w)\in C_3} 3 \langle A_u A_v A_w \rangle . \end{aligned} \tag{1b}$$

Here $V_h = \{h_\alpha\}$, $C_2 = \{(z_k, y_k^+), (z_k, y_k^-), (y_k^+, y_k^-)\}$ and $C_3 = \{(z_k, y_k^+, y_k^-)\}$, with indices k and α running as for V. A necessary condition for a set of correlations to be non-contextual is

$$\langle \chi_{\rm YO} \rangle \le 8 \quad \text{and} \quad \langle \chi_{\rm opt3} \rangle \le 25, \tag{2}$$

and any violation of these inequalities demonstrates contextuality. The prediction of quantum theory is that, for any qutrit state and under ideal conditions,

$$\langle \chi_{\rm YO} \rangle = \frac{25}{3} \approx 8.333 \quad \text{and} \quad \langle \chi_{\rm opt3} \rangle = \frac{83}{3} \approx 27.667. \tag{3}$$

Our experimental platform to test these witnesses uses a single $^{40}Ca^+$ ion confined in a surface-electrode radio-frequency trap in the setup described in [34]. The qutrit basis states are represented by three fine-structure levels in a $^{40}Ca^+$ ion: $|0\rangle = |S_{1/2}(m_j = -1/2)\rangle$ in the ground-state manifold, and $|1\rangle = |D_{5/2}(m_j = -3/2)\rangle$ and $|2\rangle = |D_{5/2}(m_j = -1/2)\rangle$ in the metastable $D_{5/2}$ manifold (FIG. 2). The two metastable states have a Zeeman-shifted energy difference $\hbar(\omega_2 - \omega_1) = (2\pi\hbar)\, 6.47$ MHz in an external magnetic field of $B = 0.385$ mT.

TABLE I. Definition and experimental parameters for the vectors $v \in V$ in the Yu-Oh set. The coefficients (a, b, c) give the directions of the rays in the real-valued three-dimensional Hilbert space (FIG. 1). In the experiment, rays are rotated onto the measurement axis (along z_1) by applying the coherent rotations in Equations (4) using the angles $\theta_v^{(1)}$, $\phi_v^{(1)}$, $\theta_v^{(2)}$, $\phi_v^{(2)}$ (see also FIG. 3). The last column shows the corresponding bit sequence from the QRNG (see text for details). If the QRNG delivers a bit sequence not present in this table, it is discarded and a new one is read in. Shorthand notations $\bar{1} = -1$ and $\theta_h^{(2)} = 2 \arctan\left(1/\sqrt{2}\right)$ were used.

v	(a, b, c)	$\theta_v^{(1)}$	$\phi_v^{(1)}$	$\theta_v^{(2)}$	$\phi_v^{(2)}$	QRNG
y_1^-	$(0, 1, \bar{1})$	π	$3\pi/2$	$\pi/2$	$\pi/2$	0001
y_2^-	$(\bar{1}, 0, 1)$	0	0	$3\pi/2$	$3\pi/2$	0010
y_3^-	$(1, \bar{1}, 0)$	$\pi/2$	$\pi/2$	0	0	0011
y_1^+	$(0, 1, 1)$	π	$3\pi/2$	$\pi/2$	$3\pi/2$	0100
y_2^+	$(1, 0, 1)$	0	0	$\pi/2$	$3\pi/2$	0101
y_3^+	$(1, 1, 0)$	$\pi/2$	$3\pi/2$	0	0	0110
h_1	$(\bar{1}, 1, 1)$	$3\pi/2$	$3\pi/2$	$\theta_h^{(2)}$	$3\pi/2$	0111
h_2	$(1, \bar{1}, 1)$	$\pi/2$	$\pi/2$	$\theta_h^{(2)}$	$3\pi/2$	1000
h_3	$(1, 1, \bar{1})$	$\pi/2$	$3\pi/2$	$\theta_h^{(2)}$	$\pi/2$	1001
h_0	$(1, 1, 1)$	$\pi/2$	$3\pi/2$	$\theta_h^{(2)}$	$3\pi/2$	1010
z_1	$(1, 0, 0)$	0	0	0	0	1011
z_2	$(0, 1, 0)$	π	$3\pi/2$	0	0	1100
z_3	$(0, 0, 1)$	0	0	π	$3\pi/2$	1101

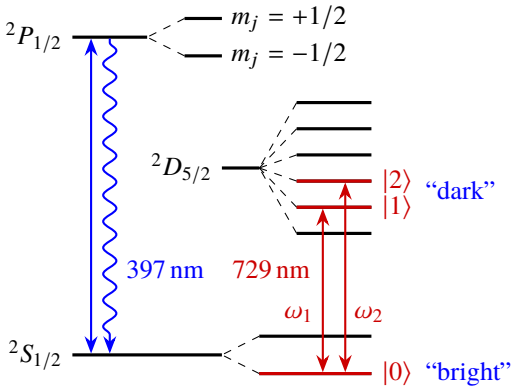

FIG. 2. (color online) Energy level diagram of the $^{40}Ca^+$ ion. Qutrit states $|0\rangle$, $|1\rangle$, and $|2\rangle$ are encoded in the highlighted fine-structure levels. Coherent rotations between them are achieved with laser pulses at 729 nm. Fluorescence measurements using an excitation laser at 397 nm project the qutrit state into either $|0\rangle$ ("bright") or the $|1\rangle, |2\rangle$-manifold ("dark").

Every experimental sequence starts with 500 µs of Doppler cooling using a 397 nm laser red-detuned approximately half a natural linewidth from resonance with the cycling transition between the $S_{1/2}$ and $P_{1/2}$ manifolds, and with close to one saturation intensity [33, 34]. This is followed by 10 µs of optical pumping to initialize the qutrit to the $|0\rangle$ state. Subsequently, measurements of the observables $\{A_v\}$ are performed, which consist of coherent rotations between the qutrit states and pro-

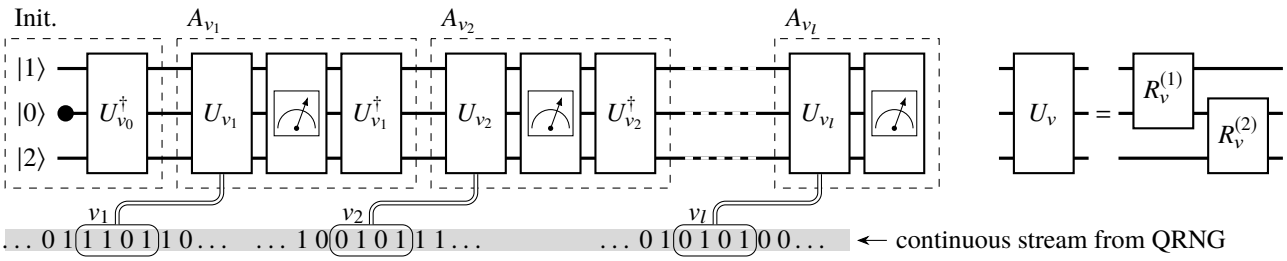

FIG. 3. Sequential measurement scheme. A subsequence starts by initializing the ion state to $|0\rangle$ and rotating it to the last ray from the previous subsequence, v_0. Every following ray measurement A_v then consists of a unitary transformation U_v rotating the ray v onto $|0\rangle$, a projective measurement, and the back rotation $U_v^\dagger$. The unitary transformations $U_v = R_v^{(2)} R_v^{(1)}$ are realized by coherent driving on the transitions between $|0\rangle$ and $|1\rangle$, $R_v^{(1)} = R^{(1)}(\theta_v^{(1)}, \phi_v^{(1)})$, and between $|0\rangle$ and $|2\rangle$, $R_v^{(2)} = R^{(2)}(\theta_v^{(2)}, \phi_v^{(2)})$. Subsequent measurement rays are determined by bit sequences from a QRNG, which are created after performing the respective previous projective measurement.

jective measurements. Coherent rotations are achieved using 729 nm laser pulses resonant with the transitions between $|0\rangle$ and $|1\rangle$ (at ω_1), and between $|0\rangle$ and $|2\rangle$ (at ω_2). Matrix representations of the rotations in the Hilbert space spanned by the basis $\{|0\rangle, |1\rangle, |2\rangle\}$ are given by

$$R^{(1)}(\theta,\phi) = \begin{pmatrix} \cos\left(\frac{\theta}{2}\right) & -\mathrm{i}e^{-\mathrm{i}\phi}\sin\left(\frac{\theta}{2}\right) & 0 \\ -\mathrm{i}e^{\mathrm{i}\phi}\sin\left(\frac{\theta}{2}\right) & \cos\left(\frac{\theta}{2}\right) & 0 \\ 0 & 0 & 1 \end{pmatrix}, \tag{4a}$$

$$R^{(2)}(\theta,\phi) = \begin{pmatrix} \cos\left(\frac{\theta}{2}\right) & 0 & -\mathrm{i}e^{-\mathrm{i}\phi}\sin\left(\frac{\theta}{2}\right) \\ 0 & 1 & 0 \\ -\mathrm{i}e^{\mathrm{i}\phi}\sin\left(\frac{\theta}{2}\right) & 0 & \cos\left(\frac{\theta}{2}\right) \end{pmatrix}. \tag{4b}$$

The angles θ and ϕ for a certain rotation (TABLE I) are controlled via the duration and phase of the corresponding laser pulse using an acousto-optic modulator. Projective measurements are realized by illuminating the ion for 160 µs with the same settings used for Doppler cooling [33]. If photons are scattered, the qutrit state is projected onto $|0\rangle$ ("bright state"); if not, the qutrit is projected onto the $D_{5/2}$ manifold ("dark states"), preserving the coherence between $|1\rangle$ and $|2\rangle$ (FIG. 2). For the bright / dark states, we register on average 18.8 / 0.7 photons through a high-numerical aperture objective on a photomultiplier tube. Thresholding single-shot photon counts at 5.5 for the 160 µs detection window allows us to distinguish bright from dark states with an estimated mean detection-error of $< 2 \times 10^{-4}$ [33].

Testing the SIC inequalities on the Yu-Oh set [13] requires projective measurements along all 13 rays (FIG. 1). By design, the fluorescence detection projects onto either the qutrit state $|0\rangle$ itself, i.e. the z_1 ray, or the plane orthogonal to it, spanned by $|1\rangle$ and $|2\rangle$. For any other observable A_v, we apply first a unitary rotation $U_v = R^{(2)}(\theta_v^{(2)}, \phi_v^{(2)})\, R^{(1)}(\theta_v^{(1)}, \phi_v^{(1)})$, which rotates v onto z_1, then fluorescence detection (followed by optical pumping of the $S_{1/2}$ population to $|0\rangle$), and finally the reverse rotation $U_v^\dagger$ (FIG. 3). Every measurement of an observable is thus uniquely determined by v and is independent of the context.

Ideally, we would perform a single long series of measurements of randomly chosen observables. In practice, we interrupt the sequence to save collected data and periodically calibrate laser frequencies and pulse times. To sustain the sequence, we take subsequences containing a minimum of 1,000 measurements, which we interrupt when the last detection projected the qutrit onto $|0\rangle$. The next subsequence then starts by initializing the qutrit to $|0\rangle$ and applying the rotation $U_{v_0}^\dagger$, with $v_0 = v_l$ the last ray from the previous sequence. In this way, all performed measurement sequences can be concatenated up to the 53 million in the present dataset [33]. The periodic reset resulting from the repeated measurements with a finite probability to find the system in $|0\rangle$ allows such long continuous sequences to be built up while restricting the propagation of unitary-rotation errors.

We randomize the sequence of measured observables using a QRNG (model Quantis from ID Quantique SA). It delivers a constant stream of random bits, from which we take groups of four and assign rays v to them (TABLE I). The random bits for an observable are created after the detection event of the previous observable (FIG. 3). In this way, if we acknowledge the randomness of the QRNG, we prevent a hypothetically conspiring ion from knowing what the context of a measurement will be [32]. Everything from the QRNG output to the pulse sequence programmed in the computer-control system is updated in real time within a 50 µs time window between unitary rotations.

In a typical sequence of 1 million measurements, we observe between two and five subsequences containing more than 55 dark measurements in a row. In a random sequence of 55 ideal measurements, we would, however, only expect such a set to occur with a probability of $(2/3)^{55} \approx 2 \times 10^{-10}$, which corresponds to a 1 % probability for it to appear once in the full set of 53 million measurements. We attribute this anomalous effect to off-resonant leakage into the states $|D_{5/2}, m_j = -5/2\rangle$ and $|D_{5/2}, m_j = +1/2\rangle$, which are long-lived dark states outside our computational Hilbert space [33]. The control system for the experiment spots these events in real time and breaks, purging the subsequence and starting a new subsequence from the same v_0 as was used for the purged subsequence.

Every data point measured for an observable A_v consists of the measurement ray v and an outcome $a = \pm 1$. From the full data set, we collect the numbers $N(A_v{=}a_1)$, $N(A_u{=}a_1, A_v{=}a_2)$, and $N(A_u{=}a_1, A_v{=}a_2, A_w{=}a_3)$, where A_u, A_v, and A_w are successive measurements in that order, for all $u, v, w \in V$ and

all $a_1, a_2, a_3 \in \{1, -1\}$. Based on these numbers, we compute the expectation values

$$\langle A_v \rangle = \frac{\sum_{a_1} a_1 N(A_v{=}a_1)}{\sum_{a_1} N(A_v{=}a_1)}, \tag{5a}$$

$$\langle A_u A_v \rangle = \frac{\sum'_{a_1,a_2} a_1 a_2 N(A_u{=}a_1, A_v{=}a_2)}{\sum'_{a_1,a_2} N(A_u{=}a_1, A_v{=}a_2)}, \tag{5b}$$

$$\langle A_u A_v A_w \rangle = \frac{\sum'_{a_1,a_2,a_3} a_1 a_2 a_3 N(A_u{=}a_1, A_v{=}a_2, A_w{=}a_3)}{\sum'_{a_1,a_2,a_3} N(A_u{=}a_1, A_v{=}a_2, A_w{=}a_3)}, \tag{5c}$$

where $\sum'$ additionally sums over all permutations of the argument list of N, i.e. the measurement order. Substituting the obtained values (FIG. 4) into the SIC witnesses in Equations (1), we find

$$\langle \chi_{\mathrm{YO}} \rangle = 8.279(4) \quad \text{and} \quad \langle \chi_{\mathrm{opt3}} \rangle = 27.357(11). \tag{6}$$

Our results violate Inequalities (2) by 69 and 214 standard deviations, which correspond to a contextual fraction of 0.167 and 0.177 respectively, out of a maximum of 0.2 in both cases [5, 33]. These deviations are solely based on statistical uncertainties, which are small due to the large number of measurements in the complete dataset. However, we believe that the significance of these violations should be penalized according to experimental imperfections and systematic errors [33], and elaborate on this issue below.

Our dataset additionally allows for evaluation of the SIC witnesses in Eqs. (1) based on the "standard approach", where measurements are repeatedly performed on specifically prepared states of the system. For this, we calculate the averages conditioned on a preceding projection onto one of the states $i \in V$. We do this for all 13 input states and observe violations of the SIC inequalities by at least 15 and 43 standard deviations, respectively [33].

Inequalities (2) are satisfied by any theory assuming noncontextuality and their violation indicates contextuality if certain underlying assumptions are satisfied. There are some such assumptions that are untestable, e.g., the assumption that observers have free will for choosing which measurement to make at any time (here implemented with a QRNG). Nevertheless, there are underlying assumptions that are (at least partially) testable. One is the assumption that measurements are sharp, i.e. they are minimally disturbing [43] and their outcomes are the same if performed repeatedly. In quantum theory, sharp measurements are represented by self-adjoint operators; the "ideal measurements" as defined by von Neumann [35] are sharp measurements. While perfect sharpness can never be fulfilled in a real experiment, we find the repeatability of our measurements (including rotations and projections) to be above 99.6 % [33]. Another assumption is compatibility between the 24 pairs of observables in E (FIG. 1b). Given compatibility, there should be i) no context signaling in the data, and ii) no influence of preceding compatible measurements on the statistics of an observable [33]. The large number of measurements comprising our dataset render statistical uncertainties very small and we are able to resolve small

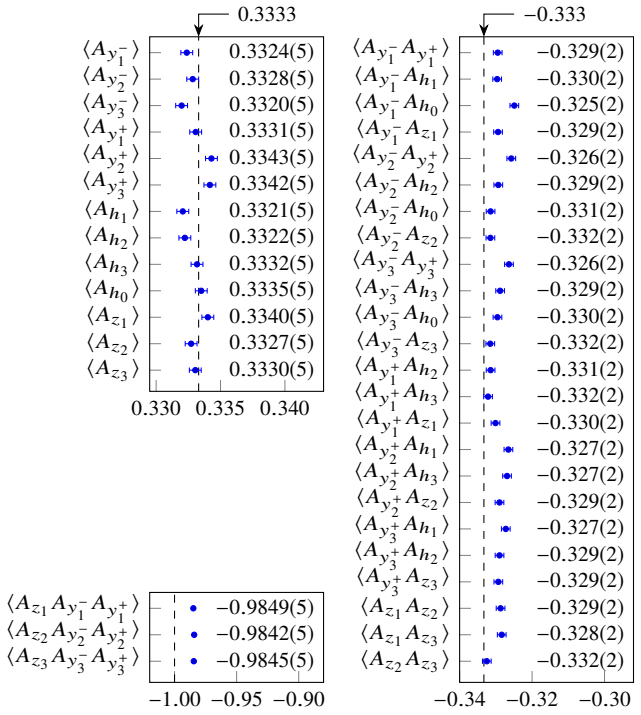

FIG. 4. Experimental results for expectation values that enter the SIC witnesses in Equations (1) (see text for details on their calculation). Error bars reflect shot noise; dashed lines represent values predicted by quantum mechanics.

systematic deviations from the ideal case in both these measures. We believe these should reflect on our results for the SIC witnesses (Eqs. (1)), but we are not aware of any standard method to account for these imperfections when evaluating SIC witnesses. There exist analytical methods to take into account such imperfections for non-contextuality inequalities for scenarios with cyclic systems in which dichotomic observables are measured in only two contexts [36]. These or other contextuality-by-default techniques [37] may serve as a starting point to account for imperfections also in the Yu-Oh scenario.

We characterize in [33] the quantum-vs-classical advantage of this experiment based on the fact that QM predictions for this system cannot be simulated with a classical trit as this would require a classical system with a substantially larger memory. Furthermore, we show that the compatibility structure between observables need not be assumed a priori, but can be inferred from the resulting statistics without invoking QM.

Beyond addressing fundamental aspects of QM, this work demonstrates a system capable of autonomously generating quantum operations, a feature desirable for a prospective quantum computer. The system concatenates hundreds of millions of coherent rotations and projective measurements, rather than repeating a finite sequence which starts with a pre-defined quantum state and consumes a resource at the end of the computation. Such long sequences of QND measurements are interesting in a range of areas including sensing and quantum computing [38]. Furthermore, the methods presented in this

paper might be generalized to multi-particle quantum systems, providing more powerful tests of fundamental physics [39–41] and addressing the question of how to optimally generate, certify and make use of quantum contextual correlations.

ACKNOWLEDGMENTS

We thank IdQuantique for the QRNG, and Matt Grau for partial checking of our data analysis and comments on the manuscript. AC thanks Matthias Kleinmann for discussions, and Mile Gu and Zhen-Peng Xu for contributions to the memory estimation in [33]. We acknowledge support from the Swiss National Science Foundation under grant no. 200021 134776, ETH Research Grant under grant no. ETH-18 12-2, and from the Swiss National Science Foundation through the National Centre of Competence in Research for Quantum Science and Technology (QSIT). The research is partly based upon work supported by the Office of the Director of National Intelligence (ODNI), Intelligence Advanced Research Projects Activity (IARPA), via the U.S. Army Research Office grant W911NF-16-1-0070. The views and conclusions contained herein are those of the authors and should not be interpreted as necessarily representing the official policies or endorsements, either expressed or implied, of the ODNI, IARPA, or the U.S. Government. The U.S. Government is authorized to reproduce and distribute reprints for Governmental purposes notwithstanding any copyright annotation thereon. Any opinions, findings, and conclusions or recommendations expressed in this material are those of the author(s) and do not necessarily reflect the view of the U.S. Army Research Office. AC acknowledges support from Project No. FIS2014-60843-P, "Advanced Quantum Information" (MINECO, Spain), with FEDER funds, the FQXi Large Grant "The Observer Observed: A Bayesian Route to the Reconstruction of Quantum Theory," and the project "Photonic Quantum Information" (Knut and Alice Wallenberg Foundation, Sweden).

Author Contributions: Experimental data were taken by FML, MM and JA, using an apparatus primarily built up by FML and JA, and with significant contributions from MM, CZ and VN. Data analysis was performed by FML, JA, JPH and AC. The paper was written by FML, JA, AC and JPH, with input from all authors. Experiments were conceived by AC, FML, JA and JPH. The authors declare that they have no competing financial interests.

[1] R. Raussendorf, Phys. Rev. A **88**, 022322 (2013).
[2] M. Howard, J. Wallman, V. Veitch, and J. Emerson, Nature **510**, 351 (2014).
[3] J. Bermejo-Vega, N. Delfosse, D. E. Browne, C. Okay, and R. Raussendorf, arXiv:1610.08529 (2016).
[4] J. Bermejo-Vega, N. Delfosse, D. E. Browne, C. Okay, and R. Raussendorf, Phys. Rev. Lett. **119**, 120505 (2017).
[5] S. Abramsky, R. S. Barbosa, and S. Mansfield, Phys. Rev. Lett. **119**, 050504 (2017).
[6] A. Cabello, V. D'Ambrosio, E. Nagali, and F. Sciarrino, Phys. Rev. A **84**, 030302 (2011).
[7] T. S. Cubitt, D. Leung, W. Matthews, and A. Winter, Phys. Rev. Lett. **104**, 230503 (2010).
[8] J. S. Bell, Physics **1**, 195 (1964).
[9] S. Kochen and E. P. Specker, Journal of Mathematics and Mechanics **17**, 59 (1967).
[10] J. F. Clauser, M. A. Horne, A. Shimony, and R. A. Holt, Phys. Rev. Lett. **23**, 880 (1969).
[11] A. A. Klyachko, M. A. Can, S. Binicioğlu, and A. S. Shumovsky, Phys. Rev. Lett. **101**, 020403 (2008).
[12] A. Cabello, Phys. Rev. Lett. **101**, 210401 (2008).
[13] S. Yu and C. Oh, Phys. Rev. Lett. **108**, 030402 (2012).
[14] G. Kirchmair, F. Zähringer, R. Gerritsma, M. Kleinmann, O. Gühne, A. Cabello, R. Blatt, and C. F. Roos, Nature **460**, 494 (2009).
[15] E. Amselem, M. Rådmark, M. Bourennane, and A. Cabello, Phys. Rev. Lett. **103**, 160405 (2009).
[16] O. Moussa, C. A. Ryan, D. G. Cory, and R. Laflamme, Phys. Rev. Lett. **104**, 160501 (2010).
[17] C. Zu, Y.-X. Wang, D.-L. Deng, X.-Y. Chang, K. Liu, P.-Y. Hou, H.-X. Yang, and L.-M. Duan, Phys. Rev. Lett. **109**, 150401 (2012).
[18] X. Zhang, M. Um, J. Zhang, S. An, Y. Wang, D.-l. Deng, C. Shen, L.-M. Duan, and K. Kim, Phys. Rev. Lett. **110**, 070401 (2013).
[19] V. D'Ambrosio, I. Herbauts, E. Amselem, E. Nagali, M. Bourennane, F. Sciarrino, and A. Cabello, Phys. Rev. X **3**, 011012 (2013).
[20] Y.-F. Huang, M. Li, D.-Y. Cao, C. Zhang, Y.-S. Zhang, B.-H. Liu, C.-F. Li, and G.-C. Guo, Phys. Rev. A **87**, 052133 (2013).
[21] G. Cañas, S. Etcheverry, E. S. Gómez, C. Saavedra, G. B. Xavier, G. Lima, and A. Cabello, Phys. Rev. A **90**, 012119 (2014).
[22] G. Cañas, M. Arias, S. Etcheverry, E. S. Gómez, A. Cabello, G. B. Xavier, and G. Lima, Phys. Rev. Lett. **113**, 090404 (2014).
[23] O. Gühne, M. Kleinmann, A. Cabello, J.-A. Larsson, G. Kirchmair, F. Zähringer, R. Gerritsma, and C. F. Roos, Phys. Rev. A **81**, 022121 (2010).
[24] M. Wajs, S.-Y. Lee, P. Kurzyński, and D. Kaszlikowski, Phys. Rev. A **93**, 052104 (2016).
[43] G. Chiribella and X. Yuan, arXiv (2014), 1404.3348v2.
[26] R. Colbeck, *Quantum and Relativistic Protocols for Secure Multi-Party Computation*, Ph.D. thesis, University of Cambridge (2007).
[27] M. Um, X. Zhang, J. Zhang, Y. Wang, S. Yangchao, D.-L. Deng, L.-M. Duan, and K. Kim, Sci. Rep. **3**, 1627 (2013).
[28] J. S. Bell, Rev. Mod. Phys. **38**, 447 (1966).
[29] A. Cabello, M. Kleinmann, and C. Budroni, Phys. Rev. Lett. **114**, 250402 (2015).
[30] A. Cabello, M. Kleinmann, and J. R. Portillo, J. Phys. A: Math. Theo. **49**, 38LT01 (2016).
[31] M. Kleinmann, C. Budroni, J.-Å. Larsson, O. Gühne, and A. Cabello, Phys. Rev. Lett. **109**, 250402 (2012).
[32] A. Peres and A. Ron, in *Microphysical Reality and Quantum Formalism*, Vol. 2, edited by A. V. der Merwe, F. Selleri, and G. Tarozzi (Kluwer, Dordrech, Holland, 1985) pp. 115–123.
[33] See Supplemental Material, which includes Refs. [42] and onward..
[34] J. Alonso, F. M. Leupold, Z. U. Solèr, M. Fadel, M. Marinelli,

B. C. Keitch, V. Negnevitsky, and J. P. Home, Nature Communications **7**, 11243 (2016).
[35] J. Neumann, *Mathematische Grundlagen der Quantenmechanik*, Grundlehren der mathematischen Wissenschaften (Springer Berlin Heidelberg, 1932).
[36] J. V. Kujala, E. N. Dzhafarov, and J.-Å. Larsson, Phys. Rev. Lett. **115**, 150401 (2015).
[37] E. N. Dzhafarov, J. V. Kujala, and V. H. Cervantes, in *Quantum Interaction*, edited by H. Atmanspacher, T. Filk, and E. Pothos (Springer International Publishing, Cham, 2016) pp. 12–23.
[38] S. Haroche, Rev. Mod. Phys. **85**, 1083 (2013).
[39] A. Cabello, E. Amselem, K. Blanchfield, M. Bourennane, and I. Bengtsson, Phys. Rev. A **85**, 032108 (2012).
[40] X. Zhan, X. Zhang, J. Li, Y. Zhang, B. C. Sanders, and P. Xue, Phys. Rev. Lett. **116**, 090401 (2016).
[41] S. Abramsky, R. S. Barbosa, N. de Silva, and O. Zapata, arXiv (2017), 1705.07310.
[42] W. M. Itano, J. C. Bergquist, J. J. Bollinger, J. M. Gilligan, D. J. Heinzen, F. L. Moore, M. G. Raizen, and D. J. Wineland, Phys. Rev. A **47**, 3554 (1993).
[43] G. Chiribella and X. Yuan, arXiv (2014), 1404.3348v2.
[44] A. Cabello, Phys. Rev. A **93**, 032102 (2016).
[45] F. M. Leupold, *Bang-bang Control of a Trapped-Ion Oscillator*, Ph.D. thesis, ETH Zurich (2015).
[46] A. Bermudez, X. Xu, R. Nigmatullin, J. O'Gorman, V. Negnevitsky, P. Schindler, T. Monz, U. Poschinger, C. Hempel, J. Home, F. Schmidt-Kaler, M. Biercuk, R. Blatt, S. Benjamin, and M. Müller, arXiv:1705.02771 (2017).
[47] D. Leibfried, R. Blatt, C. Monroe, and D. Wineland, Rev. Mod. Phys. **75**, 281 (2003).
[48] A. H. Myerson, D. J. Szwer, S. C. Webster, D. T. C. Allcock, M. J. Curtis, G. Imreh, J. A. Sherman, D. N. Stacey, A. M. Steane, and D. M. Lucas, Phys. Rev. Lett. **100**, 200502 (2008).
[49] M. Kleinmann, O. Gühne, J. R. Portillo, J.-Å. Larsson, and A. Cabello, New Journal of Physics **13**, 113011 (2011).
[50] A. Cabello, M. Gu, O. Gühne, and Z.-P. Xu, arXiv:1709.07372 (2017).
[51] A. Peres, Physics Letters A **151**, 107 (1990).
[52] N. D. Mermin, Phys. Rev. Lett. **65**, 1838 (1990).